Water Research 292 (2026) 125251

Contents lists available at ScienceDirect

Water Research

journal homepage: www.elsevier.com/locate/watres

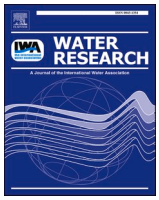

Exploring seasonal lability and fate of dissolved organic nitrogen cycling in a field-scale water filtration system

Jinxiang Cheng [a], Amy M. McKenna [b,c], Ni-Bin Chang [a,*]

[a] Department of Civil, Environmental, and Construction Engineering, University of Central Florida, Orlando, FL, USA
[b] National High Magnetic Field Laboratory, Florida State University, Tallahassee, FL, USA
[c] Department of Soil and Crop Sciences, Colorado State University, Fort Collins, CO, USA

HIGHLIGHT

- Internal cycling embedded in DON decomposition is critical for DON lability and fate.
- ZIPGEM media mix has netter DON fractional removal than CPS.
- Chemical descriptors and energetic properties help distinguish the lability of DON.

ARTICLE INFO

Keywords:
Dissolved organic nitrogen
Water filtration
Specialty adsorbents
Nitrogen removal

ABSTRACT

Dissolved organic nitrogen (DON) is a substantial yet under-managed component of aquatic nitrogen cycling, whose transformation in nature-based biogeochemical processes and engineered systems depends on molecular composition, lability, and hydrologic forcing. This paper presents the unique distribution of DON lability classes (labile, semilabile, or refractory) across fate and transport processes (removed, produced, retained) over ten sampling events in a field-scale water filtration system, linking them to molecular descriptors, thermodynamic properties, and Kendrick mass defect (KMD) connectivity. This field-scale water filtration system contains two green sorption media (specialty adsorbents) and they include zero-valent iron and perlite-based green environmental media (ZIPGEM), and a clay-perlite with sand sorption media (CPS). ZIPGEM retained predominantly refractory DON formulas (60–85%) but produced a more labile effluent pool (40–70%, the percentage of DON molecular formulas), revealing an internal molecular cycle in which aromatic and condensed DON are reconfigured into reduced, aliphatic by-products. This internal cycling was corroborated by saturation–redox zoning: retained formulas clustered within oxidizing–saturated domains, whereas produced formulas were enriched threefold in reducing–saturated regions. CPS, by contrast, exhibited labile-dominated removal and semilabile production with minimal redox partitioning. Seasonal changes further modulated these dynamics—within ZIPGEM, produced DON formulas declined from 62.1% (dry season) to 44.1% (wet season) as retained refractory DON molecular formulas increased by ~8%, coinciding with net ammonium release (–83% removal percentage) in wet season. KMD-resolved homologous sequences and tiered cycling statistics (244 internal loops, with first-level cycles of up to 33 molecules) indicated extensive redox-coupled molecular reconfiguration within ZIPGEM. Collectively, these results show that DON transformation in green sorption media is governed by hierarchical internal cycling, driven by redox-saturation interfaces and seasonal forcings, which together control the coexistence of bioavailable and refractory nitrogen in treated effluents.

1. Introduction

Nitrogen pollution is one of the most pressing challenges in global aquatic environments (Schulte-Uebbing et al., 2022), closely linked to eutrophication (Menció et al., 2023), harmful algal blooms (Wang et al., 2023), drinking water safety (Wu et al., 2021), and ecosystem imbalance (Peñuelas, and Sardans, 2022). While most research and management efforts have historically focused on inorganic nitrogen species such as

* Corresponding author.
E-mail address: nchang@ucf.edu (N.-B. Chang).

https://doi.org/10.1016/j.watres.2025.125251
Received 13 October 2025; Received in revised form 10 December 2025; Accepted 19 December 2025
Available online 24 December 2025
0043-1354/© 2025 Elsevier Ltd. All rights are reserved, including those for text and data mining, AI training, and similar technologies.

nitrate, nitrite, and ammonium, dissolved organic nitrogen (DON) represents a substantial yet often overlooked component in the nitrogen cycle. DON is ubiquitous in rivers (Kim et al., 2023; Chen et al., 2022a), lakes (Wen et al., 2022; Kurek et al., 2023), wetlands (Kurek et al., 2024), agricultural runoff (Yang et al., 2022), and wastewater effluents (Tang et al., 2021), and its molecular composition is highly complex (Hu et al., 2022), encompassing lignin-like and condensed aromatic compounds, protein- and amino sugar-like molecules, carbohydrates, tannins, lipids, and others (Li et al., 2024). These compounds exhibit wide variability in chemical properties, which directly determines their lability, fate and transport in the environment (Qu et al., 2024). The lability refers to the degree of significant changes in DON concentration or composition (Bronk et al., 2024). In this paper, the lability refers to the frequency or time scale of DON formulas in ten field sampling events at a water filtration system as a proxy (details in Section 2.3). It is noted that the interaction between DON lability and fate across different pathways remains insufficiently resolved—particularly at field-scale, where hydrologic pulses, aging of green sorption media (speciality adsorbents) for water filtration, and micro redox heterogeneity are poorly captured by laboratory reactors and therefore limit transferability of bench-scale insights. Here we leverage an event driven, field-scale dataset from a field-scale water filtration plant for testing two specialty adsorbents to interrogate these gaps. It aims to quantify how seasonality impact redistributes DON pathways externally and internally among lability pools and fates, link those patterns to molecular chemical descriptors and energetic proxies, and use ultrahigh resolution mass spectrometry, including diagnostics of Kendrick Mass Defect (KMD), to reveal internal cycling that connects lability with treatment outcomes in situ.

Even though most research and management efforts remain focused on the removal of total nitrogen and inorganic nitrogen (Paul and Banerjee, 2022; Zhou et al., 2023), with the advent of ultrahigh-resolution mass spectrometry, such as Fourier transform ion cyclotron resonance mass spectrometry (FT-ICR MS), substantial progress has been made in characterizing the molecular composition of DON (Xiao et al., 2020). Qualitative frameworks are now relatively well established (Nebbioso and Piccolo, 2013), allowing identification of major compound classes including lignin-like, aromatic, protein- and amino sugar-like, and carbohydrate-like molecules based on the Van Krevelen diagrams. However, quantitative investigations are still in their infancy, and several important knowledge gaps remain even though some recent studies have categorized DON based on treatment origin in terms of produced, shared, or removed fractions (Cui et al., 2024). There remains no established framework that integrates molecular lability (labile, semilabile, refractory) with DON fate (removed, produced, retained) in a way that directly reflects chemical reactivity and transformation potential. This study signifies several milestones. First, our work introduces a unified lability–fate–descriptor–KMD framework (Figure S1 and Supplementary note 1) to fill this gap. More importantly, such a framework is not only underpinned by high-resolution molecular characterization but also synergized KMD analysis and molecular energetics calculations to chemically delineate each DON pool to realize delicate DON molecular dynamics for why certain DON species are readily degraded while others persist via distinct molecular signatures and energy-yield characteristics for labile vs. refractory DON. Second, internal cycling processes within the DON pool are poorly understood. Paired influent (DON molecules) – effluent (DON molecules) analyses, combined with KMD, are important to identify families of molecules that undergo transformation, fragmentation, and re-emergence across treatment processes. Third, this study developed the links between molecular chemical descriptors and energetic properties with the observed fates of DON molecules that have not been systematically quantified till now. Without such integration, it remains difficult to translate molecular-level observations into indicators of effluent lability and downstream water quality risk in the nitrogen cycle. This study addressed these gaps using a quantitative framework such as these atom ratios of H/C, O/C, and N/C, as well as double bond equivalents (DBE), modified aromaticity index (AImod), nominal oxidation state of carbon (NOSC), molecular lability Index (MLB_L), and combustion enthalpy (ΔH) that integrates occurrence frequency as a proxy for lability, molecular descriptors and energetic indices for chemical descriptors-based selectivity, as well as KMD analysis for understanding of internal cycling of DON, within the paired influent–effluent context over seasons

In this context, the proposed specialty adsorbents (i.e., two new green sorption media) have emerged as promising alternatives for nutrient removal due to their low cost, renewable sources, and environmentally friendly properties (Wen et al., 2020; Valencia et al., 2020). Among them, clay–perlite–sand (CPS) and zero-valent iron–perlite–-green environmental media (ZIPGEM) have been tested in applications to treat agricultural runoff in a river corridor in Florida (Cheng et al., 2024a). These green sorption media have demonstrated satisfactory performance in removing total nitrogen and inorganic nitrogen (Cheng et al., 2024a; 2024b); however, their roles in governing the molecular-level dynamics of DON remain poorly understood. It is not known how DON is removed, produced, or retained within such media, nor how these removal processes are connected to DON lability, energetic traits, and potential internal cycling. Elucidating these aspects in representative green sorption media such as CPS and ZIPGEM is therefore critical for advancing both process optimization and risk assessment.

Accordingly, this study aims to decipher the lability and fates of DON in representative green sorption media, using CPS and ZIPGEM as model systems. By combining 21T FT-ICR MS with molecular chemical descriptors, energetic indices, and KMD analysis, we seek to establish a quantitative framework for understanding DON transformations at the molecular level. Specifically, this study addresses three interrelated questions: (i) How do different treatment media (ZIPGEM vs. CPS) and seasonal conditions (dry season vs. wet season) alter the fates of DON across lability pools (labile, semilabile, refractory)? (ii) What molecular chemical descriptors and energetic properties (e.g., H/C, O/C, N/C ratios, DBE, AImod, MLB_L, NOSC, ΔH) better distinguish the lability of DON molecules that are removed, produced, or retained during treatment? (iii) How does internal cycling within the DON pool reshape the distribution of labile fractions and molecular composition, thereby influencing effluent lability and potential DON removal in different seasons?

2. Material and methods

2.1. Experimental design and operation

The field-scale filtration experiment was set up on the southern side of Canal 23 (Fig. 1a), which is located in the St. Lucie River Basin, Florida. The experiment was positioned in such a way that it allowed for direct pumping from the canal and then the treated water would be returned downstream, which would expose this filtration plant to conditions in the watershed that change with the seasons, while also ensuring that there would not be any short circuit issue occurring at the intake. Two green sorption media were tested in this field experiment. ZIPGEM comprised 85 % sand, 5 % clay, 5 % zero-valent iron (ZVI), and 5% perlite by volume. CPS comprised 92% sand, 5% clay, and 3% perlite by volume (Fig. 1b) (Cheng et al., 2024a; 2024b).

The experimental setup was made up of four geomembrane-coated infiltration cells (Cells 1–4), arranged in parallel along the canal's edge (Cheng et al., 2024a). Every cell had dimensions of 6.67 m (22 feet) in width, 40.3 m (133 feet) in length, and a depth of 1.1 m (4 feet) for excavation. The cells were equipped with ≥40 mil high-density polyethylene, secured within a boundary trench. At each cell's base, a 0.15 m (6-inch) gravel drainage layer with 0.1 m (4-inch) perforated laterals linked to a 6-inch underdrain manifold was set up and topped with a non-woven geotextile to block media penetration. Over the gravel layer,

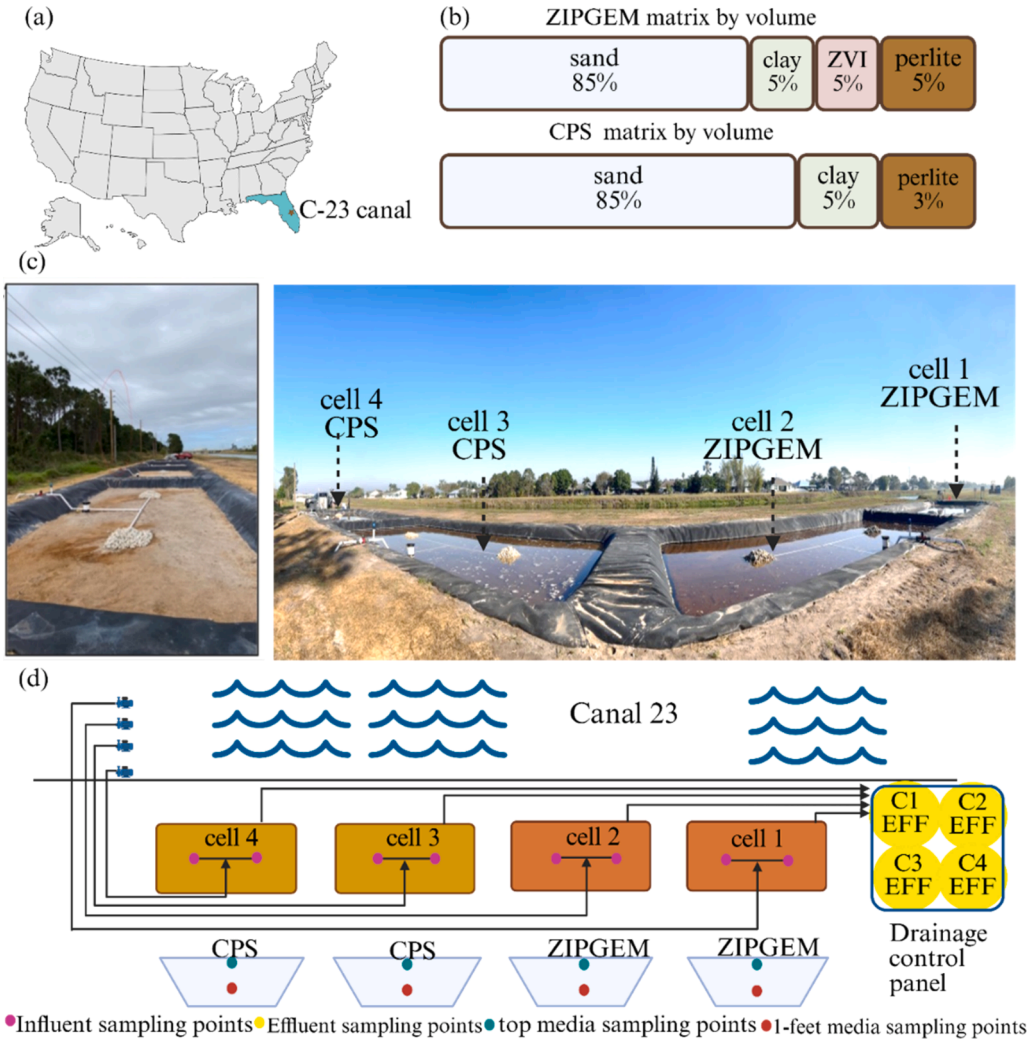

Fig. 1. Introduction of the pilot filtration system. (a) Filtration cell's location: Latitude (27°12′19.8″N) and Longitude (80°23′47.8″W). (b) media composition. (c) Panoramic view of four filter cells in the pilot plant after construction (left) and in process (right). (d) Layout of the field-scale filtration system by the C-23 Canal, constructed to investigate nutrients and algal mass removal from the canal water.

a layer of 0.6 m (2 feet) of testing medium was laid. For the purpose of facilitating duplication and comparative analysis in the same water and weather scenarios, ZIPGEM media mix was used in Cells 1 and 2, while CPS media mix was employed in Cells 3 and 4 (Fig. 1c). The detailed experimental setup can be seen in Supplementary note 2 and Figure S2.

The sampling sites were set to facilitate comparisons between influent and effluent pairs. Samples of influent grab were gathered at the bubbler manifolds, while effluent samples were obtained from specific ports on the drainage control panel, located just after the underdrain outlet of each cell (Fig. 1d). Ten manual sampling/monitoring events were conducted approximately at two-week intervals between March 1 and July 3, 2023 (Table S1). Each sampling event included manual collection of water (both influent and effluent) and media samples from each of the filtration cells, manual recording of basic water quality parameters, and maintenance of automatic water quality sensors (Table S2) (Cheng et al., 2024a). All field water sampling events were conducted as per Florida Department of Environmental Protection Standard Operating Procedures (FDEP SOP: FT1000, FS1000, FS2000 and FS2100).

2.2. DON extraction and analysis

For each sampling event, 500 mL of influent and effluent water samples were collected. Dissolved organic matter was isolated by solid-phase extraction (SPE) using Bond Elut™ PPL cartridges (200 mg, 3 mL; Agilent). Cartridges were used to remove matrix impurities and retain dissolved organic matter (DOM); retained material was eluted with methanol (MeOH) following a standard PPL protocol (Dittmar et al., 2008). All solvents were HPLC-grade (Sigma-Aldrich, St. Louis, MO). SPE eluates were diluted in MeOH to 100 ppm prior to mass spectrometric analysis. The details of SPE operation can be seen in Supplementary method 1.

High-resolution mass spectra were acquired at the National High Magnetic Field Laboratory (NHMFL; Tallahassee, FL) by negative-ion electrospray ionization (ESI) coupled to 21 Telsa FT-ICR MS. A micro-ESI source (50 μm i.d. fused-silica emitter) delivered sample at 500 nL min $^{-1}$ (Emmett et al., 1998). Typical ion source conditions were −2.8 to −3.2 kV emitter voltage, 45 % S-lens radio frequency (RF,) and 350 °C heated capillary. Analyses were performed on a custom FT-ICR MS hybrid linear ion trap fitted with a 21 Telsa superconducting solenoid magnet (Hendrickson et al., 2015). Negative ions were accumulated in an external multipole ion guide for 1–5 ms and mass-selected by adjusting the auxiliary RF between the multipole rods and end-cap electrode (Hendrickson et al., 2015; Smith et al., 2018). To optimize dynamic range and peak capacity, ions were excited to an m/z -dependent cyclotron radius, with excitation and detection on a single electrode pair (Kaiser et al., 2013). The dynamically synchronized ICR cell operated at a 6 V trapping potential (Chen et al., 2014). Time-domain

transients of 3.1 s were acquired; 100 time-domain acquisitions were averaged per spectrum. Data were collected with the Predator data station (serving excitation/detection) under transistor-transistor logic trigger control from a Thermo commercial station (Kaiser et al., 2013; Boldin and Nikolaev, 2011). The details of FT-ICR MS can be ssen in Supplementary method 2.

Mass spectra were phase-corrected (Xian et al., 2010) and internally calibrated using 10–15 oxygen-rich homologous series spanning the full mass range via the "walking" calibration procedure (Savory et al., 2011). Subsequent elemental-formula assignment and descriptor calculations (H/C, O/C, N/C, DBE, AImod, NOSC, (DBE–O)/C, MLB_L) followed the workflows detailed elsewhere in the Methods 2.3 and Supplementary note 3.

2.3. Quantitative analysis of chemical descriptors

To interrogate the compositional controls on DON decomposition, we applied a suite of chemical descriptors for every assigned formula, including atomic ratios (H/C, O/C, N/C), DBE, AImod, NOSC, (DBE–O)/C as an unsaturation/aromaticity proxy, and the MLB_L. Descriptor definitions and calculation formulas are provided in Table S4. Because the C-23 canal is the exclusive influent source, we treated the influent as a common pool across cells. Specifically, for each event we merged the formula lists from the four cells (set union at the formula level) to form a combined influent (INF). Effluents were aggregated by medium: formulas detected downstream of ZIPGEM (Cells 1–2) were merged into ZIPGEM EFF, and those downstream of CPS (Cells 3–4) into CPS EFF. Thus, throughout the paper INF denotes the universal set of influent formulas, and ZIPGEM EFF and CPS EFF denote the universal sets of effluent formulas for each medium. Where needed, event-wise results are summarized across from event 1 to event 10 (denoted as EV1–EV10 hereafter).

We restricted DON to CHON formulas (composition $C_cH_hO_oN_n$) within $H/C \leq 2.2$ and $O/C \leq 1.2$, a compositional domain consistent with natural aquatic organic matter. Exact-mass formula assignments from FT-ICR MS were categorized on the van Krevelen plane following Lin et al. (2021) (Table S3). For each assigned formula $C_cH_hO_oN_n$, we calculated a suite of elemental ratios and derived indices that capture key chemical descriptors relevant to DON lability and fate (Table S4). Basic stoichiometric ratios (H/C, O/C, N/C) describe relative hydrogenation, oxygenation and nitrogen enrichment. Double-bond equivalents (DBE) and the unsaturation index (DBE–O)/C quantify the degree of unsaturation; higher (DBE–O)/C indicates more double bonds and thus more structurally unsaturated, typically less labile, molecules. The modified aromaticity index AImod (Xu et al., 2022) and the aromaticity equivalent X_c (Zhang et al., 2022) distinguish aliphatic from aromatic and condensed-aromatic structures, with larger values indicating more aromatic character. The NOSC reflects the redox state of the carbon skeleton; higher (more positive) NOSC corresponds to more oxidized, thermodynamically more favorable substrates for microbial or abiotic reduction. Finally, we used the molecular lability index (MLB_L; fraction of formulas with $H/C > 1.5$, Zhou et al., 2024) as an integrated indicator of the overall abundance of saturated, protein- and carbohydrate-like molecules that are typically more bioavailable. Together, these descriptors allow us to interpret differences in the removed, produced, and retained DON pools in terms of shifts in saturation, aromaticity, oxidation state, and lability, rather than only in terms of formula identity. To condense molecular energetics and structure, we partitioned formulas into four trait–redox zones using the joint signs of NOSC and (DBE–O)/C including (1) Zone 1: oxidizing & unsaturated (NOSC > 0, (DBE–O)/C ≥ 0); (2) Zone 2: reducing & unsaturated (NOSC ≤ 0, (DBE–O)/C > 0); (3) Zone 3: reducing & saturated (NOSC < 0, (DBE–O)/C ≤ 0); and (4) Zone 4: oxidizing & saturated (NOSC ≥ 0, (DBE–O)/C < 0).

We distinguish labile, semilabile, and refractory DON conceptually by characteristic turnover times—seconds to weeks, months to years, and decades to millennia, respectively (Bronk et al., 2024). Operationally, because turnover cannot be measured directly at the formula level in the field, we used detection frequency across ten sequential events as a proxy: formulas detected in 1–3 events were classified as LDON (labile), those in 4–8 events as SLDON (semilabile), and those in 9–10 events as RDON (refractory). This event-resolved occurrence metric assumes that formulas that recur under varying hydrologic and redox conditions behave as persistent, refractory components, whereas formulas that appear only briefly are more rapidly turned over and thus labile. This frequency-based classification is consistent with recent FT-ICR-MS studies (Zhang et al., 2025; Chen et al., 2022b; Zhang et al., 2024; Wang et al., 2024; Wang and Cai, 2023) that use spatial or temporal ubiquity of molecular formulas as a proxy for DON persistence. Because the available sample volume was largely consumed by ultrahigh-resolution mass spectrometric analyses, additional incubation or optical assays could not be performed, and we therefore use this molecular-level proxy to operationalize lability definitions in a field setting. In terms of fate, a formula detected only in the influent and absent from the effluent of a given medium is classified as "removed," a formula detected only in the effluent and not in the corresponding influent is classified as "produced," and a formula present in both influent and effluent is classified as "retained".

We applied KMD analysis (Kim et al., 2003; Merel, 2023) to resolve homologous relationships and infer plausible transformation motifs within and across DON pools. KMD was computed using Eqs. (1)–(2): the Kendrick mass rescales exact masses by the chosen base (e.g., $-CH_2$) and the KMD is the difference between nominal and Kendrick mass. By construction, organic molecules that differ by integral multiples of a base unit share identical KMD and align into homologous series. We screened for diagnostic mass differences Δm corresponding to recurrent functional-group transfers (Table S5), including $-CH_2$, $-COO$, $-H_2$, $-OH$, $-O$, $-CO$, $-H_2O$,$-C_6H_5$ (Kim et al., 2003). Where the produced and retained DON pools exhibited series relations with the influent (or removed) pools at these Δm, we interpreted them as putative biochemical or interface-mediated transformations rather than random co-occurrence. The detailed KMD analysis can be seen in Supplementary method 3.

$$\text{Kendrick mass (F)} = (\text{observed mass}) \times \frac{\text{nominal mass (F)}}{\text{exact mass(F)}} \ldots\ldots \quad (1)$$

$$\text{KMD} = \text{nominal mass} - \text{Kendrick mass (F)} \quad (2)$$

In our workflow (Figure. S1), KMD-inferred internal cycling is constructed in two steps. First, as we presented before, for each of the ten sampling events we classify DON formulas into "removed", "produced", and "retained", based on exact-mass matching. Second, we search for KMD–based mass differences between removed and produced formulas that correspond to well-known neutral losses or gains (e.g., $\pm CH_2$, $\pm H_2O$, $\pm CO_2$), which we interpret as candidate methylation/demethylation, hydration/dehydration, carboxylation/decarboxylation and related transformations. When a formula that appears as a "product" in one event re-appears as an "influent" formula in another event and again participates in KMD-consistent mass differences, it becomes part of a multi-step loop. By chaining these links across events, we recover recurrent cycles connecting lignin-, condensed aromatic-, unsaturated hydrocarbon-, protein/amino sugar- and carbohydrate-like formulas.

The combustion enthalpy of individual DON formulas was approximated from elemental ratios as a proxy for molecular-level energy content. Following the Patel–Erickson formulation and subsequent refinements (Patel and Erickson, 1981; Battley, 1998; Popovic, 2019), the standard molar enthalpy of complete combustion (ΔH) is proportional to the number of electrons transferred to O_2 during oxidation and can be expressed as eq (3):

$$\Delta H = -114.14 \times \left(4 + \frac{H}{C} - 2\frac{O}{C}\right) \ldots\ldots\ldots \quad (3)$$

where H/C and O/C are the hydrogen-to-carbon and oxygen-to-carbon atomic ratios of the formula, respectively. ΔH is reported here in units of kJ·mol^{-1} C to normalize by carbon content. This composition-based thermodynamic index was calculated for all assigned DON formulas and used to compare the relative energy richness of removed, produced, and retained pools and of different compound classes. More negative ΔH values correspond to more reduced, energy-rich molecules, whereas less negative values indicate more oxidized, energy-poor molecules.

Relative electronic energies of representative DON molecules involved in lignin–condensed aromatic–protein/amino sugar–carbohydrate transformation pathways were computed using the AMS 2025 suite (SCM) with the DFTB engine (SCC-DFTB, DFTB3, 3ob-3-1 parameter set). PDB-matched structures were first geometry-optimized in the gas phase and then subjected to single-point energy calculations. The resulting total electronic energies (in eV per molecule) were used to compare the relative stability of intermediates along with the proposed transformation sequences. These DFTB energies are reported as relative electronic energies and are used qualitatively to illustrate the downhill trend of specific pathways; they are not directly compared numerically with ΔH (kJ·mol^{-1} C).

3. Results

3.1. DON fate across lability levels in different seasons

Segmenting DON into removed, produced, and retained pools displayed distinct lability-dependent behaviors between the two green sorption media across seasons (Fig. 2a–d). During the dry season in ZIPGEM, the removed DON was predominantly composed of semilabile

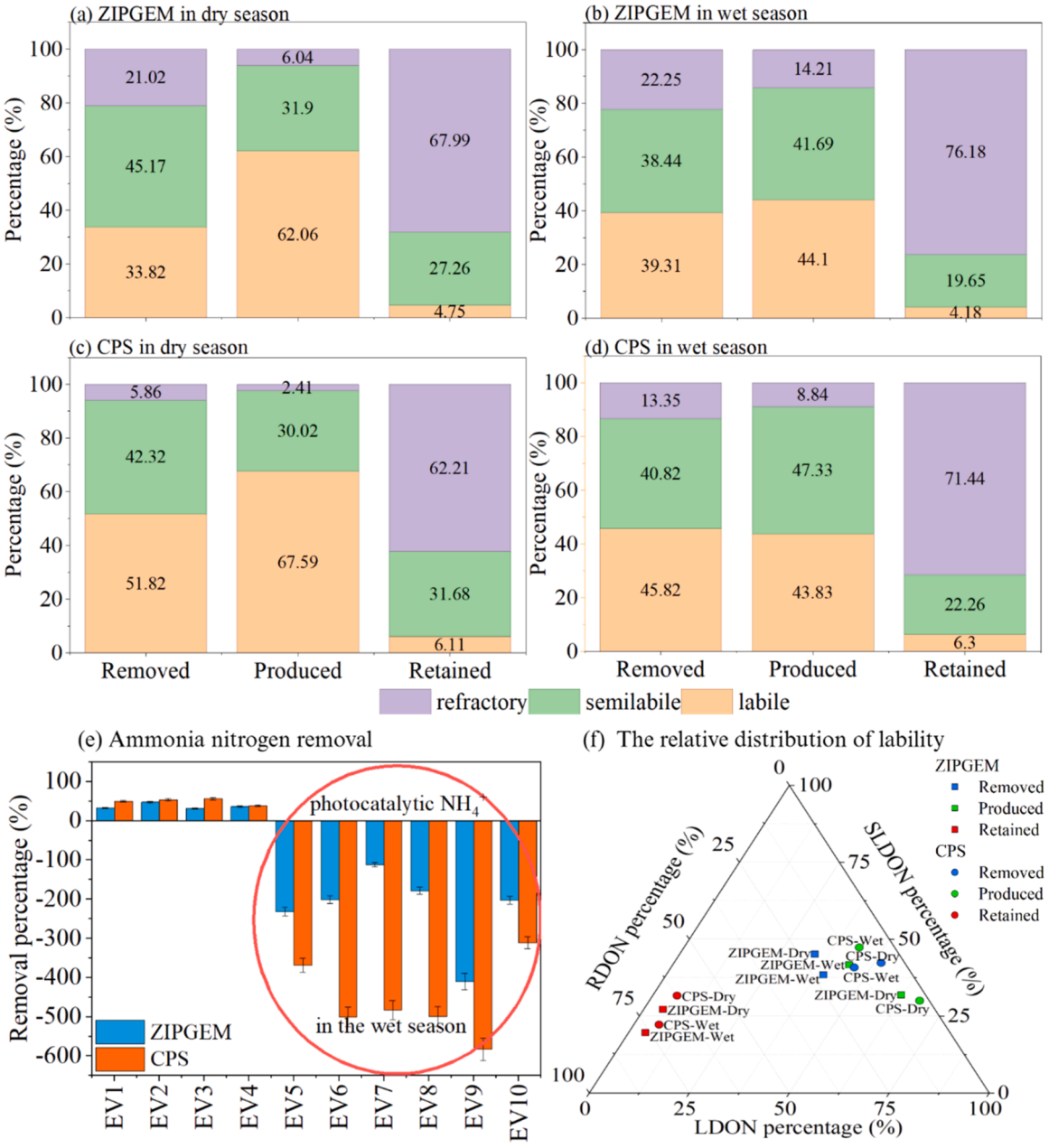

Fig. 2. Separation of dissolved organic nitrogen (DON) fates across lability pools in CPS and ZIPGEM mesocosms. The proportional contributions of labile (LDON), semilabile (SLDON), and refractory (RDON) DON in removed, produced, and retained fractions under dry and wet season (a-d). It is noted that proportions are molecule-count-weighted. (e) Seasonal ammonium removal percentages. (f) Ternary plots summarize relative LDON–SLDON–RDON distributions of removed, produced, and retained pools.

molecules (45.17 %), along with 33.82 % labile and 21.02 % refractory molecules. Conversely, there was a significant increase in labile DON in the produced pool (67.06 %), indicating a shift from semilabile and refractory precursors to more bioavailable variants. Nonetheless, the molecules retained were primarily composed of refractory DON (67.99 %), underscoring the enduring presence of compounds rich in aromatic compounds (i.e. lignin, condensed aromatic compounds) in ZIPGEM (Figure. S3). In the dry season, CPS displayed a comparable trend, albeit with significant variances: over half (51.82 %) of the removed pool was labile DON, in contrast to a mere 5.86 % of the pool that was refractory, and the produced pool had a comparable labile fraction (67.59 %), suggesting a less effective removal of refractory substances than ZIPGEM.

ZIPGEM and CPS displayed marked differences across seasons. In the case of ZIPGEM, throughout the wet season, there was a rise in the percentage of refractory DON in the retained pool from 67.99 % to 76.18 %, and a decrease in the labile portion of the pool produced from 62.06 % to 44.1 %. In the case of CPS, throughout the wet season, there was a rise in the percentage of refractory DON in the retained pool from 62.21 % to 71.44 %, and a decrease in the labile portion of the pool produced from 67.59 % to 43.83 %. Concurrently with these changes, there was a significant shift in ammonium activity. Although both media successfully removed NH_4^+ in the dry season (exceeding 80 % average removal percentage), the wet season saw a decline in the average removal percentage, dropping to –192 % in CPS and –83 % in ZIPGEM (Fig. 2e). The concentration of DON can be seen in Table S6. This reversal indicates that intensified photochemical and redox processes in the summer season not only generated new labile DON but also promoted ammonification, directly contributing to NH_4^+ accumulation in effluents.

The ternary projection of the lability composition revealed steady but differing trends across various media and seasons (Fig. 2f). Produced fractions plotted closest to the labile apex, reflecting their enrichment in LDON: in CPS, the produced pool contained 67.59 % LDON and only 2.41 % RDON in the dry season, while in ZIPGEM the labile share was lower (62.06 %) and shifted down to 44.1 % under the wet season as the semilabile fraction expanded to 41.69 %. Removed pools were positioned along the LDON–SLDON axis, with CPS consistently richer in LDON (51.82 % in dry and 45.82 % in wet) compared to ZIPGEM (33.82 % and 39.31 %, respectively). Retained fractions aggregated near the refractory vertex, with RDON comprising 62.21 % of CPS in dry season, 71.44 % in of CPS in wet season, and climbing from 67.99 % to 76.18 % in ZIPGEM from dry to wet seasons. These shifts indicate that CPS preferentially channels labile compounds into both removal and production, whereas ZIPGEM is more effective at retaining refractory material and undergoes a stronger seasonal reconfiguration from labile- to refractory-dominated fates. Therefore, these trends reveal that green sorption mediums serve dual roles as absorbers, emitters, and modifiers of DON, with the seasonal dynamics and media composition collectively determining if effluents contain bioavailable or refractory nitrogen.

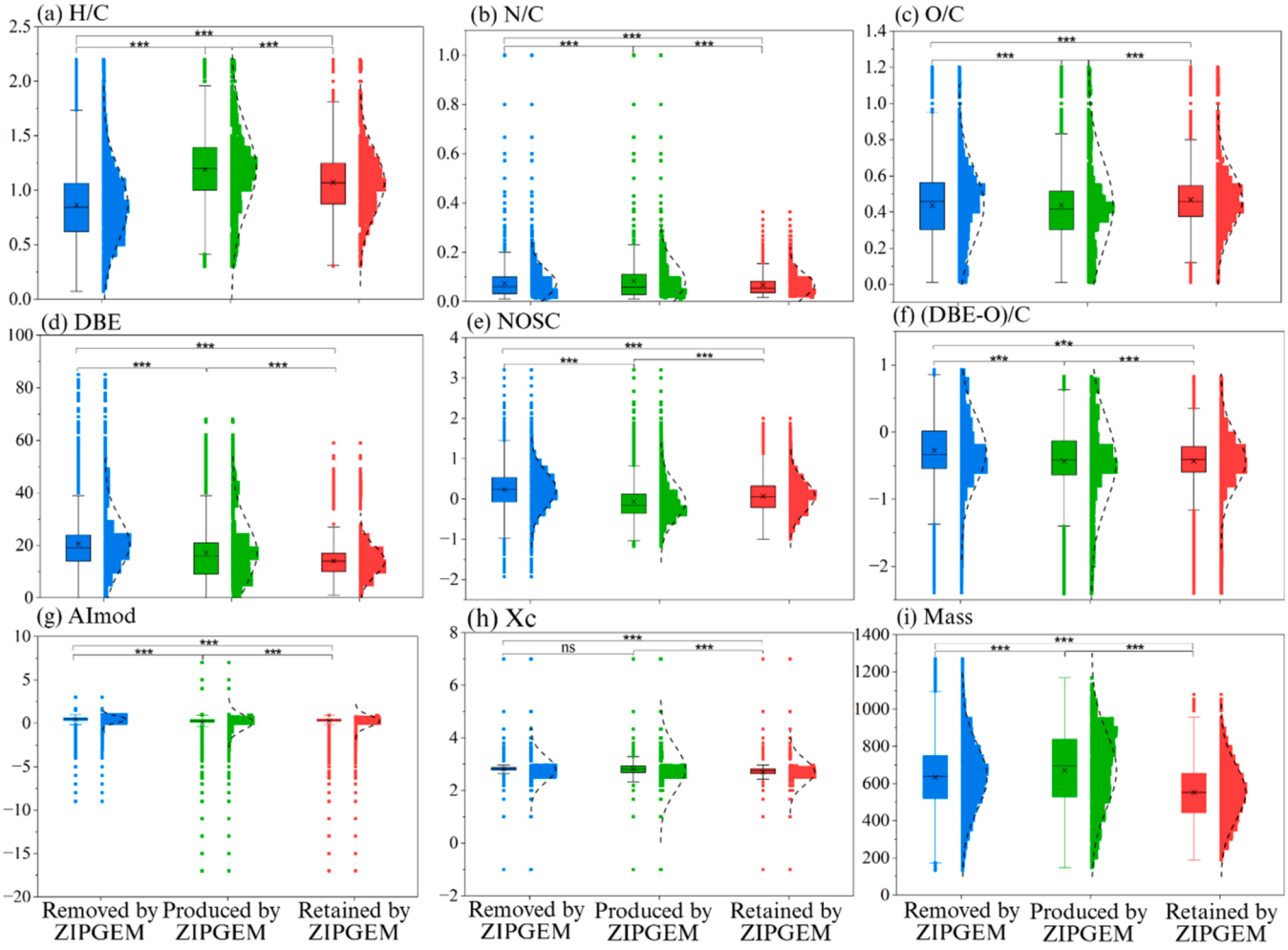

Fig. 3. Molecular chemical descriptors distributions and class-level transformations of dissolved organic nitrogen (DON) in ZIPGEM. (a) H/C, (b) N/C, (c) O/C, (d) DBE, (e) NOSC, (f) (DBE-O)/C, (g) AImod, (h) Xc, (i) Mass.

3.2. Molecular chemical descriptors and energetic properties of DON fate

Building on the lability-based separation, molecular chemical descriptors analyses revealed that DON fractions were not only redistributed among labile, semilabile, and refractory pools but also differed systematically in their chemical properties. Removed molecules carried the signatures of oxidized aromatics, produced molecules shifted toward reduced and nitrogen-enriched forms, and retained molecules concentrated refractory traits (Fig. 3a–i).

Analyzing chemical descriptor distributions statistically underscored these differences. Molecules that were removed uniformly exhibited characteristics of oxidized aromatic compounds: for ZIPGEM, lowest mean H/C (0.923), highest mean DBE (19.6), highest mean AImod (0.45), and highest mean Xc (2.86), in addition to increased (DBE–O)/C (–0.42) (Table S7), indicating enhanced unsaturation and aromatic properties. Additionally, they exhibited the greatest mean NOSC (0.34) and mean O/C (0.45), indicating a state of higher oxidation, and the lowest mean N/C (0.09), suggesting precursors low in nitrogen but abundant in oxygen. The mean molecular weight approximated 629 Da. Together, these characteristics suggest a selective removal of unsaturated, oxidized, and aromatic compounds that are less bioavailable.

Compared to those removed, the molecules produced exhibited a contrasting profile. Within ZIPGEM, the mean H/C ratio rose to 1.27, whereas mean DBE and mean AImod decreased to 16.2 and 0.10, respectively, and mean Xc fell to 2.87, indicating a decrease in aromaticity (Table S7). The mean ratio of (DBE–O)/C (–0.67) turned increasingly negative, signifying heightened saturation. The produced DON exhibited a decrease in the mean of NOSC (0.14) and the mean of O/C (0.54), yet an increase in the mean of N/C (0.11) (Table S7), indicating a trend towards reduced and nitrogen-rich substances. The mean value of MLB_L increased fourfold to 26.1, and their average molecular weight rose to approximately 651 Da, with enthalpy hitting –478.737 kJ mol^{-1}C, consistent with production of larger, energy-dense, and more bioavailable molecules such as protein/amino sugar- and carbohydrate-like species.

Retained molecules occupied an intermediate position. In ZIPGEM, the retained DON exhibited a mean H/C ratio of 1.15, mean DBE at 13.3, mean AImod at 0.31, and mean Xc at 2.75, where the mean value of (DBE–O)/C equaled –0.64, indicating a moderately saturated yet aromatic substance. The state of oxidation remained moderate (mean NOSC = 0.23, mean O/C = 0.55), with mean N/C consistently low (0.09). Compared to the molecules produced, there was a decrease in the mean value of MLB_L value (12.2) of the retained, and the average mass fell to approximately 547 Da, aligning with a partial disintegration but a buildup of smaller, resistant residues. The presence of enthalpy (–461.6 kJ mol^{-1} C) reinforced the persistence of moderately oxidized refractory structures.

Comparable trends were noted in CPS (Table S7). Molecules that were removed exhibited characteristics rich in aromatic compounds (mean DBE ≈ 19.4, mean AImod ≈ 0.39), resulting in a shift towards molecules produced rich in hydrogen and energy (mean H/C ≈ 1.16, mean MLB_L = 18.7, mean enthalpy ≈ –461.1 kJ mol^{-1} C), and the retained DON remained the most refractory group (lowest mean MLB_L = 9.8, mean enthalpy ≈ –456.9 kJ mol^{-1} C).

These chemical descriptor-based differences were mirrored in the class-level transformations visualized by the Sankey diagram (Figure. S4). For each fate category (influent, removed, produced, retained) we compiled all ΔH values and plotted their normalized kernel density functions, referred to as “enthalpy distributions” in Figure. S4. These curves therefore represent the relative frequency of formulas with a given combustion enthalpy and are used to compare how treatment shifts the thermodynamic status of the DON pool, rather than to quantify absolute energy fluxes. The removed were primarily composed of lignin- and condensed aromatic molecules with elevated enthalpy levels, while the produced molecules were abundant in protein/amino sugar- and carbohydrate-like entities moving towards lower enthalpy, aligning with the creation of reduced, bioavailable substances. The retained molecules predominantly consisted of molecules similar to lignin and tannin, linked to moderately negative enthalpy, underscoring their continued existence within medium. Together, the molecular chemical descriptor distributions and molecular class pathways demonstrate that green sorption media are not passive filters but selective processors: they preferentially remove oxidized aromatics, generate reduced labile compounds, and retain refractory DON, thereby reshaping both the chemical composition and thermodynamic landscape of effluent DON.

Collectively, the aggregated data from the distribution of chemical descriptors (Fig. 3a–i), average chemical descriptor values (Table S7), and pathways at the class level (Figure. S4) reveals that green sorption mediums function as active molecular selectors instead of mere neutral filters. They persistently remove oxidized and aromatic compounds, produce molecules which are rich in hydrogen, nitrogen, and more unstable thermodynamically, and retain resistant fractions like lignin and tannin-like entities. The diverse nature of this selectivity modifies both the chemical makeup and the energy characteristics of DON pools, shedding light on the lability patterns of effluents outlined in Section 3.1. Furthermore, the evident link between molecular classes and enthalpy gradients implies that these changes are interconnected, not singular occurrences, but components of wider reconfiguration routes, paving the way for the internal cycling mechanisms examined in Section 3.3.

3.3. Internal cycling of DON molecules revealed by KMD analysis over seasons

The KMD analysis, coupled with molecular structure verification against the Protein Data Bank (PDB), demonstrated that numerous DON molecules within ZIPGEM effluents were connected through systematic homologous series rather than existing as isolated entities (Fig. 4a). These molecules comprise one of the largest internal cycles of DON molecules among Paths A, B, and C (Fig.4b) in ZIPGEM effluents resulting in many recalcitrant DON molecules that are not labile or semilabile. Confirmed molecular formulas such as $C_{26}H_{22}N_2O_5$, $C_{25}H_{16}N_2O_2$, and $C_{24}H_{16}N_2O_4$ were linked through consistent mass differences corresponding to key reactions—hydrogenation/dehydrogenation, hydroxylation/dehydroxylation, methylation/demethylation, oxidation/reduction, and aromatization/dearomatization—representing reversible modifications among lignin-, condensed aromatic-, and unsaturated hydrocarbon-like compounds. These repeated transformations demonstrate that aromatic-rich refractory DON does not simply persist inertly but undergoes continual molecular reconfiguration, allowing its sustained presence within the treatment system.

Integration of KMD and energetic analyses revealed a hierarchical, multi-level internal cycling pattern (Figs.. 4b). The first-level cycle, consisting of bidirectional Paths A–C, forms a closed triad among lignin, condensed aromatics, and unsaturated hydrocarbons, representing the largest and most persistent internal loop in ZIPGEM. These aromatic reservoirs serve as long-lived hubs where reversible redox and substitution reactions recycle DON molecules rather than removing them. From these hubs, second- to fifth-level cycles (Paths D–G) direct molecular fluxes toward progressively more labile classes: condensed aromatics → protein/amino sugars (Path D), lignin → protein/amino sugars (Path E), lignin → carbohydrates (Path F), and protein/amino sugars → carbohydrates (Path G). Collectively, 244 interconnected cycles were detected, ranging from short 2-molecule loops to long 33-molecule chains (Table S8). First-level cycles dominated (33–30 links per loop, $n = 45$), indicating extensive internal feedback among refractory DON classes, whereas lower-level cycles (≤ 10 links) were less frequent but directed toward more bioavailable products. This network topology reveals a tiered transformation hierarchy, in which stable aromatic frameworks continually regenerate smaller, labile nitrogenous molecules while maintaining a refractory backbone. The details of 244 cycles can be seen in Table S9. It is noted that the confirmation of these

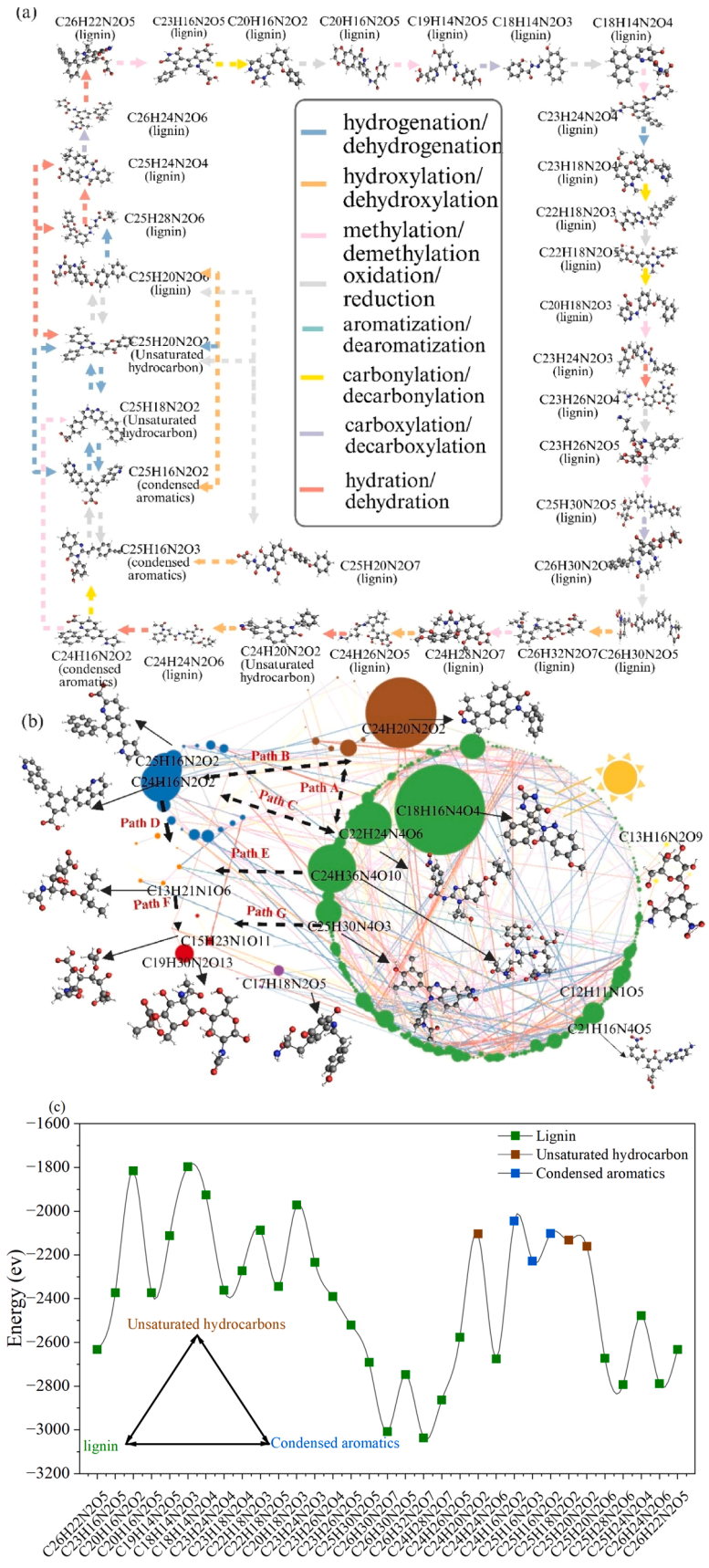

(caption on next page)

Fig. 4. The largest internal cycling of DON molecules among Paths A, B, and C in ZIPGEM effluents. (a) Kendrick Mass Defect (KMD) analysis linking validated molecular formulas (cross-checked against the Protein Data Bank, PDB) into homologous series through mass differences corresponding to reactions. (b) Network analysis of DON transformations resolved seven major pathways: three bidirectional routes (Paths A–C) interlinking lignin, condensed aromatics, and unsaturated hydrocarbons, and four unidirectional funnels (Paths D–G) channeling material into protein/amino sugar- and carbohydrate-like pools. (c) Thermodynamic profiling of DON molecules involving internal cycling.

reaction loops would require targeted experiments (e.g., laboratory incubations with ^{15}N-labeled DON, time-resolved FT-ICR-MS, or compound-specific isotope tracing) that are beyond the scope of this field study.

Thermodynamic profiling further substantiated the feasibility of these transformations (Fig. 4c). Molecules within the lignin–condensed aromatic–unsaturated hydrocarbon triad clustered at higher enthalpy values (–1800 to –2400 eV), while products along the downstream pathways occupied progressively lower energy states (–2500 to –3000 eV), forming a continuous energy gradient. Such a descending enthalpy trajectory indicates that the observed molecular conversions are energetically favorable, with each reaction step lowering the system's overall free energy and facilitating reconfiguration of DON pools. This aligns with previous FT-ICR-MS studies showing that thermodynamically downhill reactions drive DOM evolution from aromatic to aliphatic and from oxidized to reduced states during both microbial processing

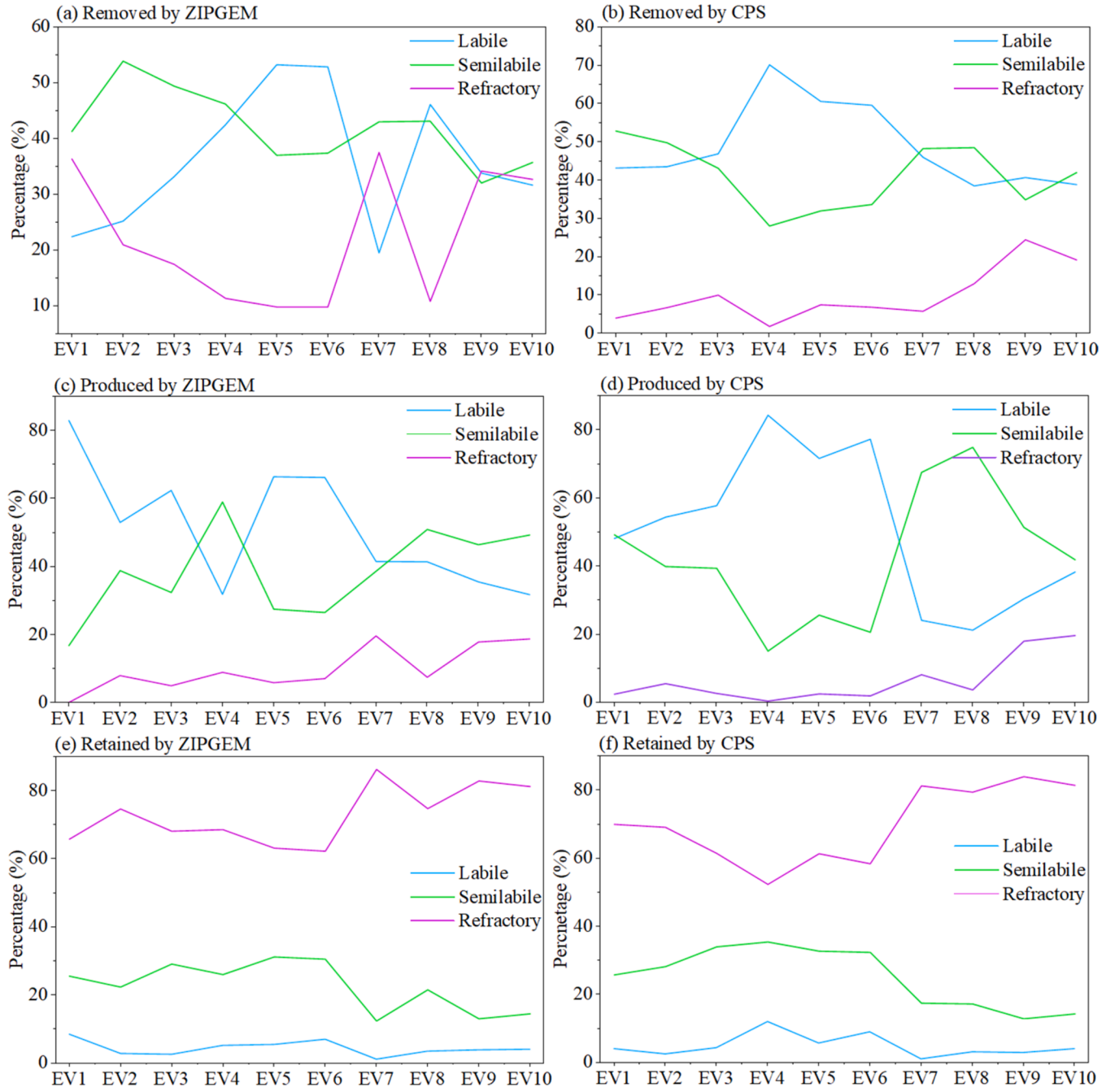

Fig. 5. Event-scale separation of DON lability across fates in two media. Percentage contributions of labile (blue), semilabile (green), and refractory (purple) DON to the removed, produced, and retained pools for ZIPGEM (a–c) and CPS (d–f) across EV1–EV10.

and abiotic redox reactions in engineered and natural aquatic systems (Zhao et al., 2021; Wang et al., 2023).

Seasonal dynamics exerted a secondary but significant influence on these internal cycles. During the dry season, the longer, higher-order cycles (first- and second-level) were predominant, suggesting sustained recycling within the aromatic domain under relatively stable hydrologic and redox conditions. In contrast, the wet season favored shorter cycles and greater flux into the labile pools, coinciding with intensified photochemical activity and ZVI-mediated redox processes under higher irradiance and increased dissolved oxygen. These seasonal shifts are consistent with the enhanced ammonium accumulation observed in Section 3.1, indicating that photochemical and biogeochemical feedback can modulate the depth and direction of DON cycling. The wet-season environment thus accelerates partial degradation of refractory compounds, while the dry season stabilizes them through extended internal cycling.

Together, Fig. 4a–c and Table S8-S9 provide convergent evidence that internal cycling constitutes a central mechanism in DON processing within ZIPGEM. Rather than following a linear removal trajectory, aromatic precursors are repeatedly reshaped through reversible KMD-defined reactions, energetically downhill conversions, and directed fluxes toward labile compounds. This continuous restructuring explains how effluents can simultaneously accumulate bioavailable DON while retaining refractory residues, complementing the trait-based selectivity described in Section 3.2. The elucidation of such multilevel, seasonally responsive internal cycles underscores the complexity of molecular nitrogen transformations in green sorption media and highlights the need to consider internal feedback when predicting effluent DON behavior and nitrogen bioavailability in tropical water-treatment systems.

4. Discussion

4.1. Seasonal–media interactions governing DON lability separation

In ZIPGEM, the removed pool fluctuates between labile and semilabile dominance, intermittently influenced by refractory DON (Fig. 5a). Nonetheless, the produced pool is primarily composed of labile DON (typically around 40–70 %), with the rate of refractory production staying low (<~15 %), except for minor spikes (Fig. 5c). In ZIPGEM, the retained pool is predominantly made up of refractory DON, usually around 60–85 % throughout various events, in contrast to labile DON, which seldom surpasses ~10 % (Fig. 5e). This suggests a robust selective fortification of refractory molecules in ZIPGEM. Consequently, the combination of refractory-dominant retention and labile-dominant production signifies internal cycling: aromatic/condensed DON becomes fixed, whereas partial transformation or microbial turnover produces more labile by-products in the effluent.

CPS exhibits an alternate equilibrium. Throughout a significant portion of the record, approximately 40–65 %, the removed pool remains labile (Fig. 5b), whereas the produced pool frequently transitions to a semilabile predominance (reaching a peak of approximately 60–70 % near the mid-series) (Fig. 5d). Nonetheless, the retained pool continues to skew the refractory (approximately 60–85 %) (Fig. 5f), though it exhibits less labile fractions compared to other pools. Together these patterns indicate that CPS preferentially takes up labile DON and regenerates semilabile DON, with less persistent enrichment of refractory retention than ZIPGEM. In other words, CPS expresses a “labile-cycle” (fast turnover with semilabile carryover), whereas ZIPGEM expresses a “refractory-cycle” (preferential immobilization of aromatic/recalcitrant DON with labile by-products).

The contrasting behaviors of CPS and ZIPGEM highlight how green sorption media determine DON fates under varying seasonal conditions. CPS consistently cycled DON through labile pools, with 51.82 % of the removed and 67.59 % of the produced fractions as LDON in the dry season, whereas ZIPGEM preferentially retained refractory DON, increasing from 67.99 % in the dry season to 76.18 % in the wet season (Fig. 2a–d). These differences are not only consistent with prior studies showing that engineered sorption media enriched with carbonaceous components tend to favor rapid microbial turnover of bioavailable nitrogen (Chang et al., 2010) but also imply integrating abiotic reduction and microbial turnover (Valencia et al., 2020; Cheng et al., 2024b) contributes to catalyzing transformations of nitrogen species.

Overlaying these media influences, the seasonal hydrological patterns significantly influenced the lability of DON. Within ZIPGEM, there was a significant reduction in the labile portion of DON produced, dropping from 62.06 % during the dry season to 44.10 % in the wet season, alongside an approximate 8 % rise in the refractory of retained pool (Fig. 2a–b). Concurrent with these changes in composition, there was an inversion in ammonium elimination, evidenced by a negative removal percentage of –83 % in ZIPGEM. This type of ammonium enrichment during the wet season mirrors findings in Uganda's tropical urban wetlands, where DON inflows, propelled by rainfall, swiftly convert into ammonium and nitrate, surpassing the denitrification potential (Byekwaso et al., 2023). Contrasting with temperate regions where chilly winters diminish microbial life (Maurice et al., 2022), tropical wetlands sustain continuous biogeochemical activity throughout the year (Adame et al., 2019), indicating that seasonal changes are more influenced by water cycles and organic matter than by temperature.

Therefore, these comparisons suggest that CPS is embedded in a “labile cycle,” repeatedly removing and regenerating bioavailable DON, whereas ZIPGEM drives a “refractory cycle,” concentrating aromatic residues. In this sense, ZIPGEM is better than CPS to remove refractory DON molecules, which also echoes the observation that ZIPGEM can remove 21.02 % refractory molecules while CPS can only remove 5.86 % refractory molecules in the dry season (Fig. 2a-and c. Such dual but divergent pathways echo broader evidence that tropical wetlands are effective year-round nutrient sinks but vulnerable to hydrologic shocks (Byekwaso et al., 2023; Adame et al., 2019). For green sorption media, this underscores the importance of adaptive management strategies—such as seasonal adjustments to hydraulic loading, vegetation harvesting, or integration with polishing units—to mitigate ammonium release and labile DON accumulation during wet seasons and sustain effluent quality.

4.2. Saturation–redox zonation and temporal consolidation of retention over seasons

By applying the NOSC– (DBE–O)/C framework to categorize formulas into four distinct “saturation–redox” areas (Figure S5 and Table S10), it's observed that ZIPGEM demonstrates a clear directional distribution of DON across fates (removed, produced, retained). Most of the retained formulas are found in Zone 4 (oxidizing, saturated; 58.12 %) (Table S10), while a significant portion is in Zone 3 (reducing, saturated; 33.29 %), suggesting a preference for immobilizing oxygenated, aliphatic formulas, then reduced aliphatic formulas, within ZIPGEM. Conversely, the produced pool moves in the direction of Zone 3 (40.47 %), with Zone 4 contributing almost equally (38.05 %). In comparison to what ZIPGEM removes (Zone 3 = 13.05 %; Zone 4 = 62.33 %), the effluent is thus concentrated with reducing-saturated substances (produced/removed enrichment for Zone 3 ≈ 3.10× for Zone 3=40.47 %/13.05 %), while it's low in oxidizing-saturated compounds (produced/removed depletion for Zone 4 ≈ 0.61× for Zone 4=38.05 %/62.33 %). Put differently, ZIPGEM generally remains oxygen-rich aliphatic DON and produces more reduced-aliphatic compounds, aligning with the redox reactions at ZVI interfaces and the internal cycling patterns inferred from KMD (Section 3.3). The contribution from Zones 1 to 2 into the retained pool is minimal (1.86 % and 6.21 %, respectively), implying that highly unsaturated classes—whether oxidizing or reducing—are either transformed toward saturated space or not preferentially captured in this medium.

In contrast, CPS demonstrates a predominance of Zone 4 in all three

fates (removed 52.01 %, produced 53.13 %, retained 61.57 %), while Zone 3′s involvement was minimal (removed 20.07 %, produced 25.16 %, retained 28.53 %). There is no strong Zone 3 enrichment in the produced pool (produced/removed ≈ 1.25× for zone 3 = 25.16 %/20.07 %), suggesting CPS predominantly converts oxygenated aliphatic formulas, lacking significant redox reformation into a smaller aliphatic space. The lability in composition enhances the findings in Section 3.1, in which CPS selectively removed LDON and produced semilabile segments, shedding light on ZIPGEM's superiority over CPS i n capturing refractory DON.

The intersample ranking of formulas retained by ZIPGEM across all ten events (Fig. 6 and Figure S6) demonstrates a systematic consolidation of retention over time. The peak of events progresses from the beginning to the end, with EV10 holding the maximum of Rank 1, succeeded by EV9 (Rank 2), EV8 (Rank 3), and EV7 (Rank 4), in contrast to early events which are concentrated in lesser ranks. The diagonal trend suggests a growing prevalence of the "consistently retained" group as the sampling event nears its end (EV8–EV10). From a mechanistic standpoint, a consistent shift is anticipated when the ability of refractory formulas to retain intensifies during operation, such as via the gradual development and aging of Fe (III) oxides due to ZVI corrosion (enhancing high affinity, ligand exchange sites) and the maturation of biofilms that improve sorptive microenvironments. This pattern corresponds with the zone-resolved findings—enhanced retention of Zone 4 in subsequent occurrences—and with the KMD derived picture of internal cycling that concentrates refractory residues on the medium while releasing more reduced, saturated by products.

Therefore, the analyses of saturation-redox zonation and event-based intersample ranking lead to a unified story: ZIPGEM selectively sequesters oxygen-abundant, carboxyl-abundant aliphatic DON, via redox-coupled processing, redirects a portion of the effluent towards reduced-aliphatic products; CPS predominantly reutilizes oxygenated aliphatic DON with limited movement across the redox axis. The comprehensive perspective offers insights into the composition and energy dynamics of the KMD-defined internal cycles outlined in Section 3.3, supporting the enhanced refractory DON captured noted in ZIPGEM

4.3. Mechanistic roots of ZIPGEM's superiority: selective retention, reactive iron interfaces, and DON internal cycling

The superior DON transformation in ZIPGEM relative to CPS arises from a synergy of selective retention, reactive iron-mediated chemistry, and molecular-level cycling. First, ZIPGEM's ZVI enables preferential capture of refractory DON. This study showed that high–molecular weight, aromatic DON fractions – the portion most resistant to biodegradation – are selectively retained by ZIPGEM whereas these refractory molecules largely escape CPS. This behavior reflects iron-driven sorption and co-precipitation processes: as ZVI corrodes to Fe(III) oxides, it creates abundant surface sites that bind and immobilize DON (Hamdi, 2025). Notably, Fe(III) oxides have a well-documented affinity for highly aromatic, oxygen-rich organic matter, effectively sequestering the less bioavailable fraction of DOM/DON (Voggenreiter et al., 2024). Enhanced coagulation studies similarly find that iron-based coagulants preferentially remove high–molecular weight humic substances (rich in organonitrogen), while smaller hydrophilic DON (e.g. amino acids or amines) remain in solution (Jathan et al., 2023). Thus, the ZVI in ZIPGEM acts as a sorbent/coagulant, stripping out the refractory DON pool via inner-sphere complexation and co-precipitation with iron hydroxides (Zhang et al., 2021). This selective retention mechanism is pivotal – it physically isolates refractory DON that would persist through media, directly contributing to higher DON retention.

Secondly, ZVI additive creates reactive iron interfaces that couple DON retention with chemical and biological transformations of nitrogen. In the moist, intermittently oxic environment of the filter, ZVI undergoes corrosion that yields Fe(II) and Fe(III) phases and elevates electron transfer reactions. These redox-active interfaces serve as microreactors where captured DON can be partially mineralized or converted (Odijk and van den Berg, 2018). For example, IFGEM (Iron Filings-based Green Environmental Media) showed >90 % NO_3^- removal, accompanied by NH_3 generation (D. Wen et al., 2020). The ZVI acts as a direct electron donor for such reactions, reducing oxidized nitrogen species and potentially cleaving nitrogen-functional groups in DON (Zou et al., 2021; He et al., 2022). At the same time, the presence of Fe(0)/Fe(II) creates localized anoxic niches (as oxygen and nitrate are consumed during corrosion) adjacent to oxic zones – ideal conditions for coupled nitrification–denitrification by microbes (Bryce et al., 2018). Indeed, iron-based green sorption media have been reported to foster a "better microbial ecology" for nutrient removal (Valencia et al., 2020), supporting autotrophic denitrifiers and heterotrophs in tandem. In ZIPGEM, this means that some organic nitrogen, once sorbed to iron hydroxides, can be microbially degraded to inorganic forms, then either volatilized as N_2 or re-assimilated. The net effect is an integrated sorption–reaction network: ZVI's corrosion products not only immobilize DON but also catalyze its breakdown. This contrasts with the passive CPS – which lacks redox capability – and explains why ZIPGEM achieves greater net loss of DON. In essence, the iron interfaces transform the filter (i.e., ZIPGEM) from an inert adsorber into a dynamic biogeochemical reactor, where nitrogen is actively cycled and removed. Iron media simultaneously remove contaminants by adsorptive sequestering and redox conversion (Robles-Lecompte et al., 2024). Here, that translates to lower residual DON because a portion of the captured organics is chemically or biologically converted to innocuous end-products within the filter.

Finally, at the molecular level, high-resolution mass spectrometry with KMD analysis provides direct evidence of internal DON cycling in ZIPGEM. Rather than the influent DON being entirely mineralized or unaltered, we detected the emergence of new organic N compounds in the effluent that were not present initially, indicating that DON undergoes partial degradation and re-synthesis inside ZIPGEM. Specifically, our FT-ICR MS data (Section 3.3) showed a shift toward formulas with lower molecular weights and higher oxygen content after treatment, along with the disappearance of certain high-KMD (hydrophobic) species. Such trends – a decrease in average m/z and KMD, and the concurrent appearance of more oxidized N-containing formulas – are a telltale signature of oxidative breakdown of larger organics into smaller products (Zhang et al., 2023). In other words, complex DON molecules captured by ZIPGEM are not simply held inertly; a fraction is broken into fragments or oxidized to new compounds, which remain as DON in modified form. This phenomenon is consistent with known DOM transformations in biologically active systems: microbes can metabolize large recalcitrant molecules into smaller units and even facilitate re-polymerization ("self-assembly") into new macromolecules (Xu and Guo, 2018). The internal production of different CHON species in ZIPGEM – as visualized by KMD series– underscores that the filter mediates a closed-cycle processing of organic nitrogen. Refractory DON is first retained and partially degraded (yielding, for instance, oxidized intermediates or ammonium); some of those intermediates may then be assimilated into microbial biomass or recondensed into new stable organics, rather than immediately exiting as DIN. Such cycling explains why the total DON transformation is higher: ZIPGEM effectively turns over the DON pool, converting a portion to removable forms. Supporting studies have likewise observed that treatment processes can alter DOM/DON composition significantly, for example by generating highly oxidized molecules while eliminating others (Zhang et al., 2023). In our case, the KMD analysis confirms that ZIPGEM's performance is not just a simple one-time capture of organics, but a continual internal transformation – a mechanism absent in the non-reactive CPS.

In summary, ZIPGEM outperforms CPS in DON transformation by acting on DON in multiple interlinked ways. The iron-mediated sorption targets the most persistent DON fractions, preventing their escape; the redox-active iron interfaces then enable chemical reduction and foster microbial processes to transform and remove nitrogen; and at the

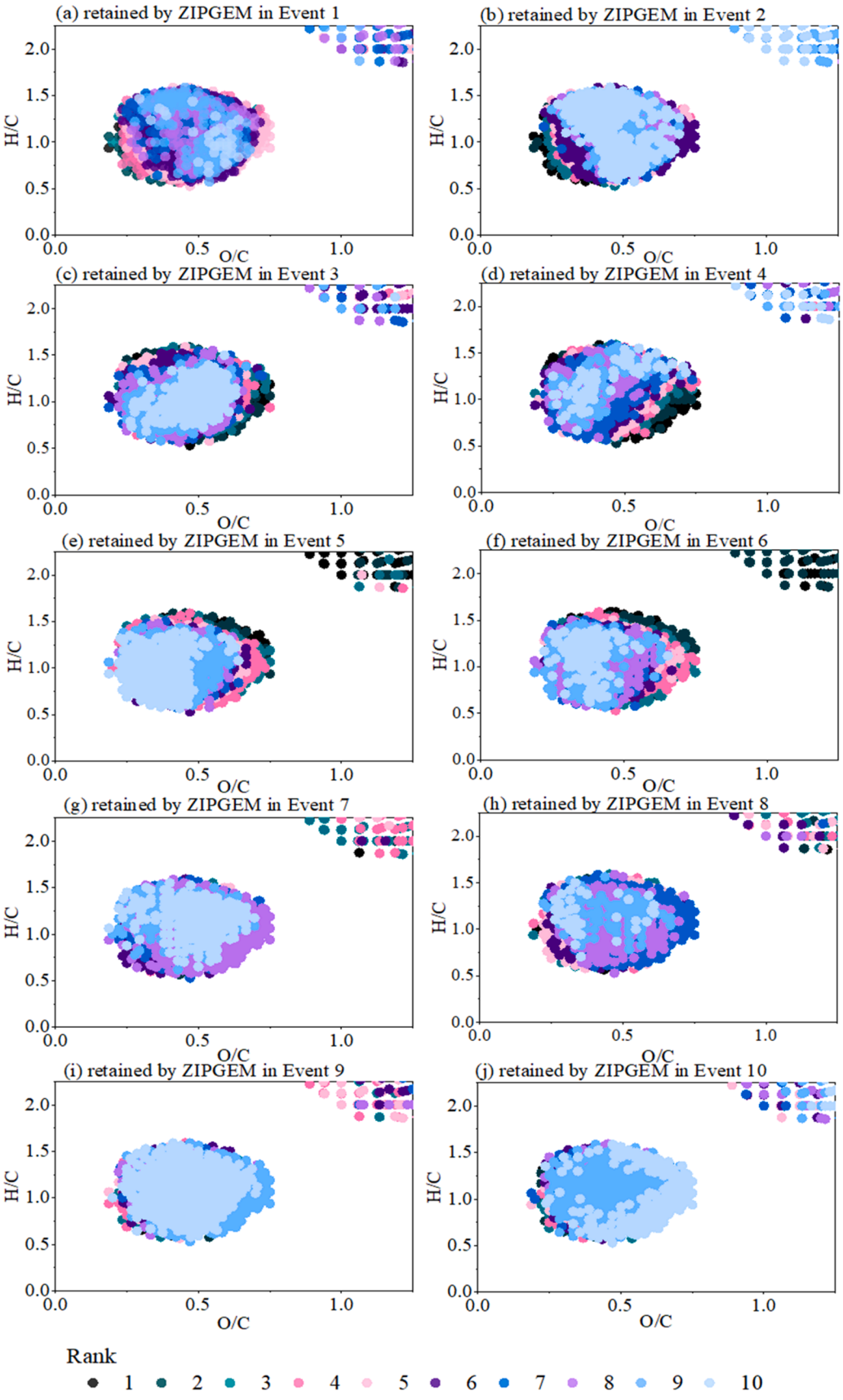

Fig. 6. the inter-sample ranking analysis for molecules retained by ZIPGEM in each event.

molecular scale, internal cycling breaks down and restructures DON, as evidenced by the altered formula patterns. These mechanisms reinforce one another – for instance, selective sorption extends the contact time of DON with reactive iron, enhancing transformations, and the byproducts of those transformations (e.g. ammonium or low-weight organics) can be further processed or retained. Such a cohesive, multi-faceted removal process is characteristic of ZIPGEM and explains its marked DON removal efficacy. By selectively retaining refractory DON, actively converting it at iron interfaces, and recycling nitrogen species internally, ZIPGEM achieves a level of DON attenuation that far exceeds that of a conventional sorptive medium (Voggenreiter et al., 2024; Jathan et al., 2023). Such mechanistic understanding not only validates ZIPGEM's superiority in our experiments but also exemplifies a broader principle: coupling physicochemical retention with reactive transformations can dramatically improve the removal of otherwise persistent nutrient pollutants (Wen et al., 2020). The present analysis, grounded in both our molecular evidence and literature precedent, thus provides a robust, critical explanation for why the ZIPGEM system excels at DON management. It underscores the importance of engineered iron interfaces and internal carbon–nitrogen cycling in achieving rigorous DON removal, a finding of significant interest for advancing stormwater and wastewater treatment technologies.

5. Conclusion

This field-scale, event-driven study indicates how the combined influences of media composition and seasonal hydrology control the lability, molecular fate, and internal cycling of DON in green sorption systems. By integrating bulk lability classifications with molecular descriptors, thermodynamic indices, and ultrahigh-resolution FT-ICR-MS fingerprints driven by high magnetic field, we link microscale compositional changes to broader patterns of DON behavior in two contrasting media. The parallel evaluation of two contrasting green sorption media (ZIPGEM and CPS) shows that differences in physicochemical reactivity and hydrologic regime are reflected in which types of DON molecules are preferentially removed, retained, or produced, even though per-formula mass fluxes are not explicitly resolved. This integrative framework closes a key bench-to-field gap in understanding nitrogen cycling within nature-based treatment technologies, showing how sorptive, redox-active media can simultaneously remove oxidized aromatic nitrogen, generate reduced labile products, and sustain hierarchical internal cycling under dynamic conditions. Across ten sampling events from dry to wet seasons, ZIPGEM consistently sequestered refractory DON—the retained pool was typically ~60–85% refractory and <10% labile—while its produced pool was labile-dominant (~40–70%). CPS showed the converse pattern: labile-heavy removal (~40–65%) and frequent semilabile-dominant production (~60–70% mid-series), with a refractory-skewed but less enriched retained pool. Seasonality amplifies these contrasts. In ZIPGEM, the labile share of produced DON fell from 62.06% (dry) to 44.10% (wet), while the refractory share of retained rose by ~8 percentage points, coincident with reversal of NH_4^+ removal (−83%) during wet season. CPS in the dry season persistently cycled labile DON (LDON making up 51.82 % of removed and 67.59 % of produced fractions). Together, the data resolves dual but divergent pathways: a refractory cycle in ZIPGEM (preferential immobilization of aromatic/recalcitrant DON with labile byproducts) versus a labile cycle in CPS (rapid turnover with semilabile carryover), with hydrologic forcing as the principal seasonal modulator. We interpret these contrasts as medium-specific regimes of DON selection and transformation in formula space, rather than as fully quantified differences in nitrogen flux performance. Positioning formulas in NOSC–(DBE–O)/C space showed that ZIPGEM retained molecules cluster in oxidizing–saturated (Zone 4, 58.12 %) with a secondary reducing–saturated (Zone 3, 33.29 %) contribution, whereas produced formulas are enriched in Zone 3 relative to what ZIPGEM removes (40.47 % vs 13.05 %; ~3.1× enrichment) and depleted in Zone 4 (38.05 % vs 62.33 %; ~0.61×). This trait–redox zonation indicates selective stabilization of oxygenated, carboxyl-rich aliphatic DON on iron phases and generation of more reduced, saturated products in the effluent. By contrast, CPS exhibits Zone 4 dominance across removed/produced/retained (52.01 %/53.13 %/61.57 %) with only modest Zone 3 participation (20.07 %/25.16 %/28.53 %), indicating muted repatterning across redox/unsaturation axes.

The KMD analysis revealed homologous series and coherent transformation motifs in ZIPGEM, demonstrating interface-mediated, redox-coupled internal cycling: refractory, oxygenated aliphatic molecules are immobilized, while partial transformations yield more reduced, saturated by-products. An intersample ranking of formulas retained in all events showed a "march of maxima" from early to late events (EV7→EV10), indicating progressive consolidation of retention capacity—consistent with ZVI corrosion producing/aging Fe(III) (oxyhydr) oxides and biofilm maturation. We emphasize that these internal cycles are inferred from compositional patterns and KMD relationships and should be regarded as hypothesized pathways that require targeted laboratory validation (e.g., isotope-labeling experiments) to confirm at the reaction level.Overall, by uniting lability segmenting, chemical descriptor analysis, saturation–redox zoning, and KMD diagnostics at field scale, we provide a coherent framework for interpreting DON behavior under variable hydrology in green sorption media. While we do not derive per-formula flux budgets, the consistent compositional patterns across events suggest that iron-rich media tend to concentrate refractory DON while generating labile by-products. These insights may help inform the design and seasonal operation of nature-based treatment systems in tropical and subtropical settings where hydrologic variability, rather than temperature, dominates short-term nitrogen processing.

CRediT authorship contribution statement

Jinxiang Cheng: Writing – original draft, Methodology, Investigation, Formal analysis, Data curation. **Amy M. McKenna:** Validation, Investigation, Formal analysis, Data curation. **Ni-Bin Chang:** Writing – review & editing, Validation, Supervision, Project administration, Methodology, Funding acquisition, Conceptualization.

Declaration of competing interest

The authors declare that they have no known competing financial interests or personal relationships that could have appeared to influence the work reported in this paper.

Acknowledgement

The authors acknowledge financial support from the Florida Department of Environmental Protection (Award ID: INV 008). A portion of this work was performed at the National High Magnetic Field Laboratory ICR User Facility, which is supported by the National Science Foundation Division of Chemistry and Division of Materials Research through DMR-2128556 (previous grant number DMR-1644779), and the State of Florida.

Supplementary materials

Supplementary material associated with this article can be found, in the online version, at doi:10.1016/j.watres.2025.125251.

Data availability

Data will be made available on request.

References

Adame, M.F., Franklin, H., Waltham, N.J., Rodriguez, S., Kavehei, E., Turschwell, M.P., Ronan, M., 2019. Nitrogen removal by tropical floodplain wetlands through denitrification. Mar. Freshw. Res. 70 (11), 1513–1521.

Boldin, I.A., Nikolaev, E.N., 2011. Fourier transform ion cyclotron resonance cell with dynamic harmonization of the electric field in the whole volume by shaping of the excitation and detection electrode assembly. Rapid Commun. Mass Spectrom. 25 (1), 122–126.

Bronk, D.A., Sipler, R.E., Letscher, R.T., McCarthy, M.D., 2024. Dissolved organic nitrogen. In: Hansell, D.A., Carlson, C.A. (Eds.), Biogeochemistry of Marine Dissolved Organic Matter (3rd ed., pp. 343–404). Academic Press.

Bryce, C., Blackwell, N., Schmidt, C., Otte, J., Huang, Y.M., Kleindienst, S., Kappler, A., 2018. Microbial anaerobic Fe (II) oxidation–ecology, mechanisms and environmental implications. Env. Microbiol 20 (10), 3462–3483.

Byekwaso, F., Weigelhofer, G., Kaggwa, R., Kansiime, F., Langergraber, G., Hein, T., 2025. Tropical wetlands as nature-based solutions to remove nutrient and organic inputs from stormwater discharge and wastewater effluent in urban environments. Water 17 (12), 1821.

Chang, N.B., Hossain, F., Wanielista, M., 2010. Filter media for nutrient removal in natural systems and built environments: I—Previous trends and perspectives. Env. Eng. Sci 27 (9), 689–706.

Chen, T., Beu, S.C., Kaiser, N.K., Hendrickson, C.L., 2014. Note: optimized circuit for excitation and detection with one pair of electrodes for improved Fourier transform ion cyclotron resonance mass spectrometry. Rev. Sci. Instrum. (6), 85.

Chen, S., Xie, Q., Su, S., Wu, L., Zhong, S., Zhang, Z., Fu, P., 2022a. Source and formation process impact the chemodiversity of rainwater dissolved organic matter along the Yangtze River Basin in summer. Water Res. 211, 118024.

Chen, M., Xu, J., Tang, R., Yuan, S., Min, Y., Xu, Q., Shi, P., 2022b. Roles of microplastic-derived dissolved organic matter on the photodegradation of organic micropollutants. Journal of hazardous materials 440, 129784.

Cheng, J., Odeh, M., Lecompte, A.R., Islam, T., Ordonez, D., Valencia, A., Chang, N.B., 2024b. Simultaneous removal of nutrients and biological pollutants via specialty absorbents in a water filtration system for watershed remediation. Environ. Pollut. 349, 123903.

Cheng, J., Robles-Lecompte, A., McKenna, A.M., Chang, N.B., 2024a. Deciphering linkages between DON and the microbial community for nitrogen removal using two green sorption media in a surface water filtration system. Chemosphere 357, 142042.

Emmett, M.R., White, F.M., Hendrickson, C.L., Shi, S.D.H., Marshall, A.G., 1998. Application of micro-electrospray liquid chromatography techniques to FT-ICR MS to enable high-sensitivity biological analysis. J. Am. Soc. Mass Spectrom. 9 (4), 333–340.

Hamdi, M.F., 2025. Advanced remediation of toxic materials using zero-valent iron nanoparticles: a comprehensive review. Water Air Soil Pollut. 236 (12), 1–29.

He, C.S., Ding, R.R., Chen, J.Q., Zhou, G.N., Mu, Y., 2022. Enhanced reductive reactivity of zero-valent iron (ZVI) for pollutant removal by natural organic matters (NOMs) under aerobic conditions: correlation between NOM properties and ZVI activity. Sci. Total Environ. 802, 149812.

Hendrickson, C.L., Quinn, J.P., Kaiser, N.K., Smith, D.F., Blakney, G.T., Chen, T., Beu, S. C., 2015. 21 Tesla Fourier transform ion cyclotron resonance mass spectrometer: a national resource for ultrahigh resolution mass analysis. J. Am, Soc, Mass Spectrom 26 (9), 1626–1632.

Hu, A., Choi, M., Tanentzap, A.J., Liu, J., Jang, K.S., Lennon, J.T., Wang, J., 2022. Ecological networks of dissolved organic matter and microorganisms under global change. Nat. Commun. 13 (1), 3600.

Jathan, Y., Pagilla, K.R., Marchand, E.A., 2023. Understanding the influence of dissolved organic nitrogen characteristics on enhanced coagulation performance for water reuse. Chemosphere 337, 139384.

Kaiser, N.K., McKenna, A.M., Savory, J.J., Hendrickson, C.L., Marshall, A.G., 2013. Tailored ion radius distribution for increased dynamic range in FT-ICR mass analysis of complex mixtures. Anal. Chem. 85 (1), 265–272.

Kim, M.S., Lim, B.R., Jeon, P., Hong, S., Jeon, D., Park, S.Y., ki Yoon, J., 2023. Innovative approach to reveal source contribution of dissolved organic matter in a complex river watershed using end-member mixing analysis based on spectroscopic proxies and multi-isotopes. Water Res. 230, 119470.

Kim, S., Kramer, R.W., Hatcher, P.G., 2003. Graphical method for analysis of ultrahigh-resolution broadband mass spectra of natural organic matter, the van Krevelen diagram. Anal. Chem. 75 (20), 5336–5344.

Kurek, M.R., Garcia-Tigreros, F., Nichols, N.A., Druschel, G.K., Wickland, K.P., Dornblaser, M.M., Spencer, R.G., 2023. High voltage: the molecular properties of redox-active dissolved organic matter in northern high-latitude lakes. Env. Sci. Technol 57 (23), 8617–8627.

Kurek, M.R., Wickland, K.P., Nichols, N.A., McKenna, A.M., Anderson, S.M., Dornblaser, M.M., Spencer, R.G., 2024. Linking dissolved organic matter composition to landscape properties in wetlands across the United States of America. Glob. Biogeochem. Cycles 38 (5) e2023GB007917.

Li, L.P., Jiao, X.Y., Peng, S., Wei, D.B., Jin, Y.C., Wang, C.S., Liu, X.H., 2024. Exploring the variations in molecular characteristics of dissolved organic matter driven by aquaculture types. Water Res. 266, 122355.

Lin, Y., Wang, L., Xu, K., Huang, H., Ren, H., 2021. Algae biofilm reduces microbe-derived dissolved organic nitrogen discharges: performance and mechanisms. Env. Sci. Technol. 55 (9), 6227–6238.

Maurice, N., Pochet, C., Adouani, N., Pons, M.N., 2022. Role of seasons in the fate of dissolved organic carbon and nutrients in a large-scale surface flow constructed wetland. Water 14 (9), 1474.

Menció, A., Madaula, E., Meredith, W., Casamitjana, X., Quintana, X.D., 2023. Nitrogen in surface aquifer-coastal lagoons systems: analyzing the origin of eutrophication processes. Sci. Total Environ. 871, 161947.

Merel, S., 2023. Critical assessment of the Kendrick mass defect analysis as an innovative approach to process high resolution mass spectrometry data for environmental applications. Chemosphere 313, 137443.

Nebbioso, A., Piccolo, A., 2013. Molecular characterization of dissolved organic matter (DOM): a critical review. Anal. Bioanal. Chem. 405 (1), 109–124.

Odijk, M., van den Berg, A., 2018. Nanoscale electrochemical sensing and processing in microreactors. Annu. Rev. Anal. Chem. 11 (1), 421–440.

Paul, D., Banerjee, A., 2022. Technologies for biological and bioelectrochemical removal of inorganic nitrogen from wastewater: a review. Nitrogen 3 (2), 298–313.

Peñuelas, J., Sardans, J., 2022. The global nitrogen-phosphorus imbalance. Science 375 (6578), 266–267.

Qu, L., Dahlgren, R.A., Gan, S., Ren, M., Chen, N., Guo, W., 2024. Spatial variation of anthropogenic disturbances within watersheds determines dissolved organic matter composition exported to oceans. Water Res. 262, 122084.

Robles-Lecompte, A., Cheng, J., McKenna, A.M., Chang, N.B., 2024. Linking pattern shifts of dissolved organic nitrogen fractional removal with microbial species richness in a cascade upflow biofiltration process. Water Res. 264, 122130.

Savory, J.J., Kaiser, N.K., McKenna, A.M., Xian, F., Blakney, G.T., Rodgers, R.P., Marshall, A.G., 2011. Parts-per-billion Fourier transform ion cyclotron resonance mass measurement accuracy with a "walking" calibration equation. Anal. Chem. 83 (5), 1732–1736.

Schulte-Uebbing, L.F., Beusen, A.H., Bouwman, A.F., De Vries, W., 2022. From planetary to regional boundaries for agricultural nitrogen pollution. Nature 610 (7932), 507–512.

Smith, D.F., Podgorski, D.C., Rodgers, R.P., Blakney, G.T., Hendrickson, C.L., 2018. 21 tesla FT-ICR mass spectrometer for ultrahigh-resolution analysis of complex organic mixtures. Anal. Chem. 90 (3), 2041–2047.

Tang, G., Li, B., Zhang, B., Wang, C., Zeng, G., Zheng, X., Liu, C., 2021. Dynamics of dissolved organic matter and dissolved organic nitrogen during anaerobic/anoxic/oxic treatment processes. Bioresour. Technol. 331, 125026.

Valencia, A., Ordonez, D., Wen, D., McKenna, A.M., Chang, N.B., Wanielista, M.P., 2020. The interaction of dissolved organic nitrogen removal and microbial abundance in iron-filings based green environmental media for stormwater treatment. Env. Res. 188, 109815.

Voggenreiter, E., Schmitt-Kopplin, P., ThomasArrigo, L., Bryce, C., Kappler, A., Joshi, P., 2024. Emerging investigator series: preferential adsorption and coprecipitation of permafrost organic matter with poorly crystalline iron minerals. Environ. Sci. Process. Impacts 26 (8), 1322–1335.

Wang, H., Bouwman, A.F., Van Gils, J., Vilmin, L., Beusen, A.H., Wang, J., Ran, X., 2023. Hindcasting harmful algal bloom risk due to land-based nutrient pollution in the Eastern Chinese coastal seas. Water Res. 231, 119669.

Wen, D., Chang, N.B., Wanielista, M.P., 2020. Assessing nutrient removal in stormwater runoff for urban farming with iron filings-based green environmental media. Sci. Rep. 10 (1), 9379.

Wen, Z., Shang, Y., Song, K., Liu, G., Hou, J., Lyu, L., He, D., 2022. Composition of dissolved organic matter (DOM) in lakes responds to the trophic state and phytoplankton community succession. Water Res. 224, 119073.

Wu, J., Bian, J., Wan, H., Ma, Y., Sun, X., 2021. Health risk assessment of groundwater nitrogen pollution in Songnen Plain. Ecotoxicol. Env. Saf. 207, 111245.

Xian, F., Hendrickson, C.L., Blakney, G.T., Beu, S.C., Marshall, A.G., 2010. Automated broadband phase correction of Fourier transform ion cyclotron resonance mass spectra. Anal. Chem. 82 (21), 8807–8812.

Xiao, K., Abbt-Braun, G., Horn, H., 2020. Changes in the characteristics of dissolved organic matter during sludge treatment: a critical review. Water Res. 187, 116441.

Xu, H., Guo, L., 2018. Intriguing changes in molecular size and composition of dissolved organic matter induced by microbial degradation and self-assembly. Water Res. 135, 187–194.

Xu, J., Zhou, P., Zhang, C., Yuan, L., Xiao, X., Dai, L., Huo, K., 2022. Striding the threshold of photocatalytic lignin-first biorefining via a bottom-up approach: from model compounds to realistic lignin. Green Chem. 24 (14), 5351–5378.

Yang, Y.Y., Tfaily, M.M., Wilmoth, J.L., Toor, G.S., 2022. Molecular characterization of dissolved organic nitrogen and phosphorus in agricultural runoff and surface waters. Water Res. 219, 118533.

Zhang, D., Dong, S., Zhang, A., Chen, L., Yu, Z., Wang, Q., Chu, W., 2021. Catalytic hydrolysis: a novel role of zero-valent iron in haloacetonitrile degradation and transformation in unbuffered systems. Sci. Total Environ. 801, 149537.

Zhang, L., Fan, X., Dong, T., Song, Z., Wang, Y., Peng, Y., Yang, J., 2023. ZVI-mediated high-rate nitrogen removal from fulvic acid (FA)-containing wastewater by anammox: revealing the genomic and molecular level mechanisms. ACS ES&T Eng. 3 (9), 1286–1296.

Zhang, S., Dong, Z., Shi, J., Yang, C., Fang, Y., Chen, G., Tian, C., 2022. Enzymatic hydrolysis of corn stover lignin by laccase, lignin peroxidase, and manganese peroxidase. Bioresour. Technol. 361, 127699.

Zhou, T., Guo, J., Liu, Q., Liu, Y., Wu, W., Wang, Y., Peng, Y., 2024. DOM and DON transformation in full-scale wastewater treatment plants: comparison of autotrophic and heterotrophic nitrogen removal units. Chem. Eng. J. 479, 147810.

Zhou, Y., Zhu, Y., Zhu, J., Li, C., Chen, G., 2023. A comprehensive review on wastewater nitrogen removal and its recovery processes. Int. J. Env. Res. Public Health 20 (4), 3429.

Zou, S., Chen, Q., Liu, Y., Pan, Y., Yao, G., Pan, Z., Lai, B., 2021. The capacity and mechanisms of various oxidants on regulating the redox function of ZVI. Chin. Chem. Lett. 32 (6), 2066–2072.